Available online at www.sciencedirect.com
SCIENCE DIRECT®

Dynamics of Atmospheres and Oceans
38 (2005) 147–171

dynamics of atmospheres and oceans

www.elsevier.com/locate/dynatmoce

The effect of idealized water waves on the turbulence structure and kinetic energy budgets in the overlying airflow

A. Rutgersson[a,b,*], P.P. Sullivan[a]

[a] *National Center for Atmospheric Research, Boulder, CO 80307, USA*
[b] *Department of Earth Sciences, Meteorology, Uppsala University, Villav 16, 752 36 Uppsala, Sweden*

Received 14 May 2004; received in revised form 1 October 2004; accepted 1 November 2004
Available online 2 February 2005

Abstract

The influence of an idealized moving wavy surface on the overlying airflow is investigated using direct numerical simulations (DNS). In the present simulations, the bulk Reynolds number is $Re = 8000$ ($Re = U_0h/v$; where U_0 is the forcing velocity of the flow, h the height of the domain and v the kinematic viscosity) and the phase speed of the imposed waves relative to the friction velocity, i.e., the wave age varies from very slow to fast waves. The wave signal is clearly present in the airflow up to at least 0.15λ (where λ is the wave length) and is present up to higher levels for faster waves. In the kinetic energy budgets, pressure transport is mainly of importance for slow waves. For fast waves, viscous transport and turbulent transport dominate near the surface. Kinetic energy budgets for the wave and turbulent perturbations show a non-negligible transport of turbulent kinetic energy directed from turbulence to the wave perturbation in the airflow. The wave-turbulent energy transport depends on the size, tilt, and phase of the wave-induced part of the turbulent Reynolds stresses.

According to the DNS data, slow waves are more efficient in generating isotropic turbulence than fast waves.

Despite the differences in wave-shape as well as in Reynolds number between the idealized direct numerical simulations and the atmosphere, there are intriguing similarities in the turbulence structure.

* Corresponding author. Tel.: +46 18 471 2523; fax: +46 18 551 124.
E-mail address: anna.rutgersson@met.uu.se (A. Rutgersson).

0377-0265/$ – see front matter
doi:10.1016/j.dynatmoce.2004.11.001

Important information about the turbulence above waves in the atmosphere can be obtained from DNS—the data must, however, be interpreted with care.

Keywords: DNS; Turbulent kinetic energy budget; Moving surface waves; Fast waves

1. Introduction

The influence of a moving water surface on the atmospheric turbulence is a research area of large interest. There is a fundamental difference between an atmospheric boundary layer over land and over sea, since the water surface moves and interacts with the overlying air in response to atmospheric forcing. Due to difficulties in making measurements over the open ocean, large uncertainties still remain concerning air–sea interaction. As measurement techniques are refined and models improved, further information about the physics of the interaction between the atmosphere and ocean surface can be obtained.

The situation over the sea can be divided into two regimes with quite different features. The most investigated regime is slow waves (a young sea with growing waves). This regime is important, for example, in wave and ocean modeling, and impacts the development of severe weather in the atmosphere. The mechanisms of the wind–wave growth are still not fully understood. One example is that the measured wave growth data obtained in the open ocean show relatively large scatter (Plant, 1982), this scatter is due to a large number of reasons including the non-linear behaviour of wave–wave interaction as well as uncertainties in the measurements. The measured values are generally higher than predictions from models (Mastenbroek et al., 1996; Belcher and Hunt, 1998).

The situation with fast waves (an old sea or swell) is even less investigated and understood. From a climatological point of view, this situation is of interest since waves traveling faster than the wind are a common feature over the ocean and they can have a large impact on the total air–sea exchange from a global perspective. There are indications from measurements that the situation with very fast waves is significantly different than has been previously assumed (Donelan et al., 1997; Drennan et al., 1999; Smedman et al., 1999). Interesting features found when very fast waves are present include persistent negative wind gradients, as reported by Rutgersson et al. (2001).

In the review by Belcher and Hunt (1998), the physical processes present in turbulent flow over waves are described and calculations based on analytical and computational models are compared. There are a variety of Reynolds averaged numerical models of varying complexity used to predict turbulent flow over wavy surfaces. Predictions from these models depend on the type of closure scheme with second-order closure models generally producing better agreement with field data than lower order closures (Mastenbroek et al., 1996; Li et al., 2000). Wave growth predictions are generally lower than estimates from experimental data and the downwind phase shift of the pressure and velocity perturbations is largely underestimated. It is also likely that Reynolds number effects need to be included in models describing processes over the ocean surface (Harris et al., 1996; Meirink and Makin, 2000).

Recently, direct numerical simulations (DNS) have been used to investigate turbulent airflow over a wavy surface for neutral (Sullivan et al., 2000) and stratified (Sullivan and McWilliams, 2002) conditions. These types of simulations have the advantage of simulating turbulence directly without any parameterisations or assumptions of the behaviour of the smaller scales. The investigations show general agreement with results from other types of models. The structure of the turbulence depends on the waves mainly in the region $kz < 1$ (where k is wave number and z the height above the surface) and for those simulations the turbulent momentum flux is altered by as much as 40% by the waves. Wave growth from the DNS is in reasonable agreement with field data and second-order closure models, in spite of the differences in Reynolds number. The present paper is a continuation of these two investigations with particular focus on the turbulence structure and kinetic energy budgets of the turbulent and wave perturbation in the air. There have been few other DNS studies of the airflow over a wavy surface; for example, Cherukat et al. (1998) used DNS to investigate flow over a stationary wavy wall. Spalart (1988) describes the turbulence structure and presents kinetic energy budgets for DNS of flow over a smooth flat surface.

The turbulent kinetic energy budgets over moving waves have also been investigated in several laboratory experiments (Hussain and Reynolds, 1970; Hsu et al., 1981; Kawamura and Toba, 1988). Most of these experiments use fairly well-developed waves (or slightly growing) and cover a limited range of wave conditions. Coherent wave perturbations can also be generated by physical processes other than a moving surface (for example, stratified layers in the atmosphere) (Liu and Merkine, 1976; Papavassiliou and Hanratty, 1997). In these studies, the interaction between wave components and turbulence is shown to be important and different from what might be expected.

In the present investigation, we analyze DNS of a plane Couette flow over a moving wavy surface at a Reynolds number lower than is generally found in laboratory studies or in the outside atmosphere. The turbulence is however well developed and the effective surface roughness is in the transitional regime between smooth and rough. Only neutral conditions are considered.

In Section 2, the problem design and numerical aspects of the DNS are briefly described. The structure of the turbulence, as evidenced by turbulence statistics and kinetic energy budgets, is presented in Section 3. Parameters used in Reynolds stress modeling are also evaluated with the DNS data, but these results will be presented in a future paper. The applicability of the present results to atmospheric flows is discussed in Section 4.

2. Problem formulation

2.1. DNS formulation

The flow investigated is a three-dimensional, turbulent, viscous, Couette flow over a series of two-dimensional water waves (Fig. 1). In the simulations, x is aligned with the flow direction, y is parallel to the waves and z is vertical from the wave crests. The external forcing of the flow is through a constant velocity U_0 imposed at $z = h$, where h is the height of the computational domain.

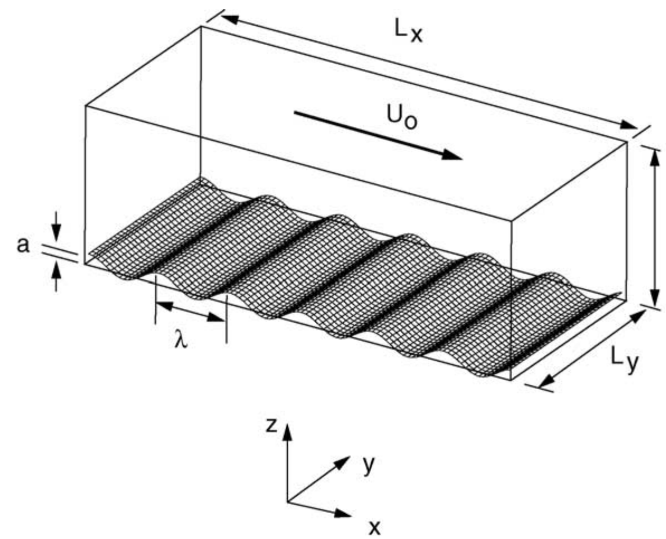

Fig. 1. Sketch of 3D Couette flow driven by velocity U_0 over a moving boundary of wavelength λ (wave number is $k=2\pi/\lambda$), phase speed c and amplitude a. The domain is $(L_x, L_y, h) = (6, 4, 1)\lambda$. Surface grid is shown with less resolution than is used in the computations.

The governing equations for this flow are the Navier–Stokes equations:

$$\begin{aligned} &\frac{\partial u_i}{\partial t} + \frac{\partial u_i u_j}{\partial x_j} = \frac{\partial p}{\partial x_i} + \frac{1}{Re}\frac{\partial^2 u_i}{\partial x_j \partial x_j} \\ &\frac{\partial u_j}{\partial x_i} = 0 \end{aligned} \tag{1}$$

where u_i $(i=1, 2, 3)=(u, v, w)$ are Cartesian velocity components and p the pressure. Length, time, velocity and pressure are made non-dimensional by h, h/U_0, U_0 and ρU_0^2, respectively. Also, the properties of the wave are made non-dimensional by h and U_0. Hence, when we refer to wind speed or phase speed of the wave, it is understood that they are made non-dimensional by U_0. Velocity and length scales normalized by wall variables (i.e., u_*, v/u_*, where u_* is friction velocity and v the kinematic viscosity) are indicated by $()^+$. The numerical method used to solve the system of equations as well as further details of the system setup is described in Sullivan et al. (2000).

2.2. Wave experiments

For our experiments, we chose a Reynolds number large enough for fully developed turbulence ($Re = U_0 h/v = 8000$). The corresponding wall Reynolds number ($Re* = u_* h/v$) is about 130. In the simulations, $(N_x, N_y, N_z) = (144, 96, 96)$ grid points are used. The vertical spacing $k\Delta z$ varies from 0.005, near the walls, to about 0.7, in the middle of the channel. There are six waves in the x-direction and, thus, 24 grid points per waveform. The wave is assumed to be a two-dimensional, periodic, deep-water gravity wave with wavelength λ, phase speed c, amplitude a and wave slope $ak = a2\pi/\lambda$. The wave slope is small enough to prevent flow separation, $ak = 0.1$. The simulations are integrated for more than 15,000

Table 1
Statistics of wave and critical-layer parameters for the six simulations

ak	c/u_*	$u_* \times 10^2$	z_0^+	kz_{cr}	z_{cr}^+
0.0	0.0	3.13	0.17	–	–
0.1	0.0	3.21	0.22	–	–
0.1	3.91	3.20	0.60	0.14	5.71
0.1	7.84	3.19	0.71	0.29	11.8
0.1	16.2	3.08	0.39	3.01	118.0
0.1	22.7	3.08	0.27	5.90	232.6

time steps (which is at least 300 large-scale, tU_0/h, time units). The stationarity of the flow was investigated looking at time series of the surface stress at the upper boundary. Only data after stationarity is reached were used. The statistics were obtained by spatial and temporal averaging using 30 three-dimensional data volumes spanning the simulation period. Increasing the number of volumes further had no effect on the statistics.

The boundary wave-shape z_{bdy} is represented by:

$$z_{\text{bdy}}(x) = a \cos kx(1 - ak \cos kx) = a \cos kx - \tfrac{1}{2}a^2k \cos 2kx - \tfrac{1}{2}a^2k \quad (2)$$

This differs slightly from a pure sinusoidal wave and produces flatter crests and deeper troughs (Weng et al., submitted for publication). However, for these small values of ak, the departure from a pure sinusoidal wave is small.

In the present work, six simulations are analyzed: a flat surface (serves as a baseline), a stationary wavy surface, and four cases with moving waves, see Table 1. The various cases differ by wave age (c/u_*), they range from young (very slow moving) to old (fast moving) waves. For young waves $c/u_* < c/u_{*|\text{tr}}$, the critical value corresponding to the transition to a mature sea is $c/u_{*|\text{tr}} \approx 14$ (Sullivan et al., 2000). This value is lower than its counterpart measured in laboratory studies and in the atmosphere where $c/u_{*|\text{tr}} \approx 25$, corresponds to fully-grown waves. In Table 1, the roughness Reynolds number (z_0^+) is also presented. Kitaigorodskii and Donelan (1984) analyzed a large number of observations over the ocean and found that the transitional regime from a smooth to rough surface occurs between $0.1 < z_0^+ < 2.2$, which covers a larger portion of the oceanic conditions (approximately when the wind speed is between $2.8\,\text{ms}^{-1}$ and $7.5\,\text{ms}^{-1}$). With this definition of the surface roughness, our DNS data is in the lower part of the transitional regime and thus possibly comparable to oceanic conditions.

2.3. Analysis procedures

One of the goals of this investigation is to identify wave-effects on the turbulence in the airflow. This can be done by decomposing any fluctuating quantity into mean, wave-induced and turbulent parts (Hussain and Reynolds, 1970):

$$f(x, y, z, t) = \bar{f}(z) + \tilde{f}(x, z) + f'(x, y, z, t) \quad (3)$$

where $\bar{f}(z)$, $\tilde{f}(x,z)$ and $f'(x,y,z,t)$ are ensemble, wave-correlated and turbulent components, respectively. We define the phase average $\langle f(x,z)\rangle$ as an average over (y,t) and periodically averaged over x with wavelength λ, thus $\tilde{f} = \langle f \rangle - \bar{f}$. In the following analysis, f will denote the total fluctuation of any fluctuating quantity (i.e., $f = \tilde{f} + f'$). Mean flow variables are identified by upper case symbols ($F = \bar{f}$).

In the presence of moving waves, the average flow direction near the surface is opposite to the direction of the flow above a certain height, as required by the surface boundary conditions. The height of the reversed flow is the height of the critical layer, z_{cr} (Belcher and Hunt, 1998). The mean critical layer in the Cartesian framework for the cases where a critical layer is present are given in Table 1 in both non-dimensional distance from the surface, kz_{cr}, and in terms of a wall variable, z^+_{cr}. There is a debate whether the critical layer influences the airflow dynamics or not. Kudryavtsev et al. (2001) states that the critical layer has only kinematical influences while Komen et al. (1994) attributes the majority of wave growth to critical layers. Recent work by Hristov et al. (2003) provides evidence that critical layers can be found in field measurements. For the present data and for slow-wave cases, it was shown in Sullivan et al. (2000), that the critical layer interacts with near-surface turbulence and critical layer dynamics are of significant importance.

The computational grid in the DNS uses a surface-fitted coordinate system. It is possible to do analysis using these coordinates, as is partly done in Sullivan et al. (2000) and in some wind-tunnel experiments (Hsu et al., 1981). In most ocean experiments, however, a Cartesian frame is used since it is easier to use a stationary measuring platform. In the present work, we interpolate fields from the surface-fitted coordinate system onto a flat Cartesian grid, with the lowest grid point just touching the top of the wave crests. The results depend slightly on the coordinate system used but analysis show that the main results and conclusions in this work are also valid for a surface-fitted coordinate system.

3. Results

3.1. Turbulence statistics

In Sullivan et al. (2000), total variances are shown to be very different for varying wave age. To investigate whether these differences are in the wave-induced or turbulent perturbations, the respective variances are analyzed separately. Vertical profiles of variances of the horizontal and vertical velocity components for wave-induced and turbulent parts are shown as function of non-dimensional distance from the surface (kz) in Fig. 2. The wave correlated contribution to the variances is significant in the region $kz < 1$, and is largest for very fast waves. For slow waves it is smaller, more so, for the vertical variances. There are small wave-induced horizontal and vertical variances also for the stationary wavy surface. For the turbulent perturbations, the slow waves act to reduce variances in the horizontal direction but increase it in the vertical direction compared to the flat surface. With stationary waves, turbulence is significantly larger in the horizontal direction compared to the flat surface. Turbulent perturbations are reduced in both horizontal and vertical directions for fast waves. Thus, we have a significant influence on both wave-induced and turbulent variances

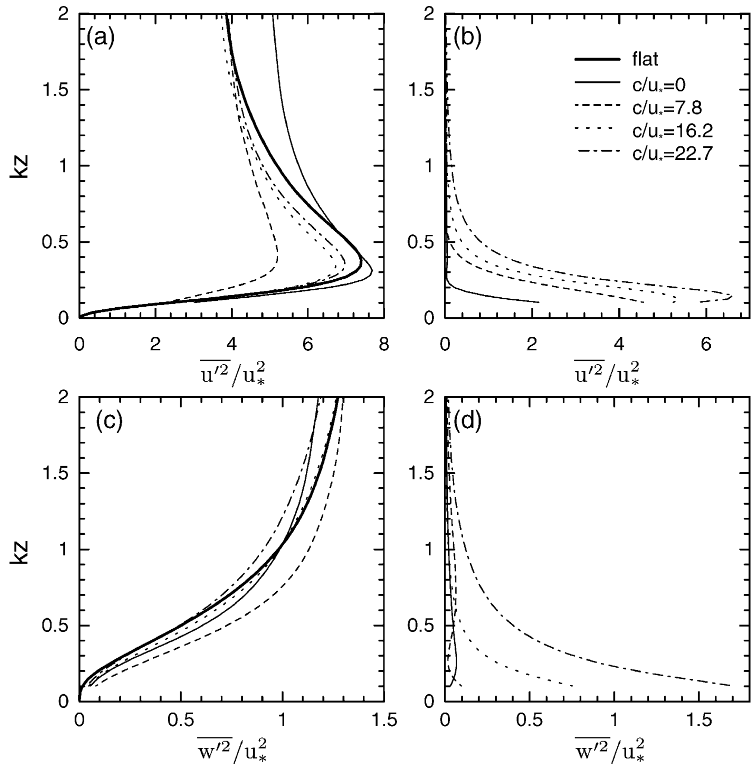

Fig. 2. Vertical profiles of the average horizontal velocity variances: (a) and (b), and vertical variances: (c) and (d). In (a) and (c), the turbulent contribution is shown, and in (b) and (d), the wave-induced contribution to the variances is shown (wave-induced and turbulent contributions are separated according to Eq. (3)).

that depend on the state of the waves. The wave-induced variances are larger for faster waves and reach to higher levels.

The vertical profile of the root-mean-square turbulent pressure ($\overline{p^2}^{1/2}$) is shown in Fig. 3a and b for the turbulent and wave-induced parts, respectively. The wave-induced pressure perturbation is large near the surface, especially for very fast waves. The wave contribution to the pressure fluctuation is smallest when the waves are closest to fully-grown ($c/u_* = 16.2$) and larger for stationary, slower and faster waves. For the fast-wave cases, there is a large increase near the surface, probably due to the surface orbital velocities. For all cases, the turbulent part of the pressure perturbation is increased near the surface compared to the flat case. The increase is largest for the slow-wave case, and the perturbation remains large well above the surface.

In Fig. 3c and d, profiles of vertical transport of pressure perturbation are shown for different cases. The pressure transport term in the turbulent kinetic energy budget is further analyzed in Section 3.2. The smallest vertical flux of wave-induced pressure perturbation $\overline{\tilde{w}\tilde{p}}$ occurs for the most mature sea and increases in magnitude for both slower and faster moving waves. For very fast waves, $\overline{\tilde{w}\tilde{p}}$ is surprisingly small considering the very large values of $\overline{\tilde{w}^2}$ and $\overline{\tilde{p}^2}$ in Figs. 2d and 3b. This can be explained by Fig. 4 which shows spatial (x, z) contours of the wave-correlated fields ($\tilde{w}/u_*$, $\tilde{p}/u_*^2$ and $\tilde{w}\tilde{p}/u_*^3$) for the very fast-wave case. The magnitude of the absolute value of the wave-integrated data is displayed in the

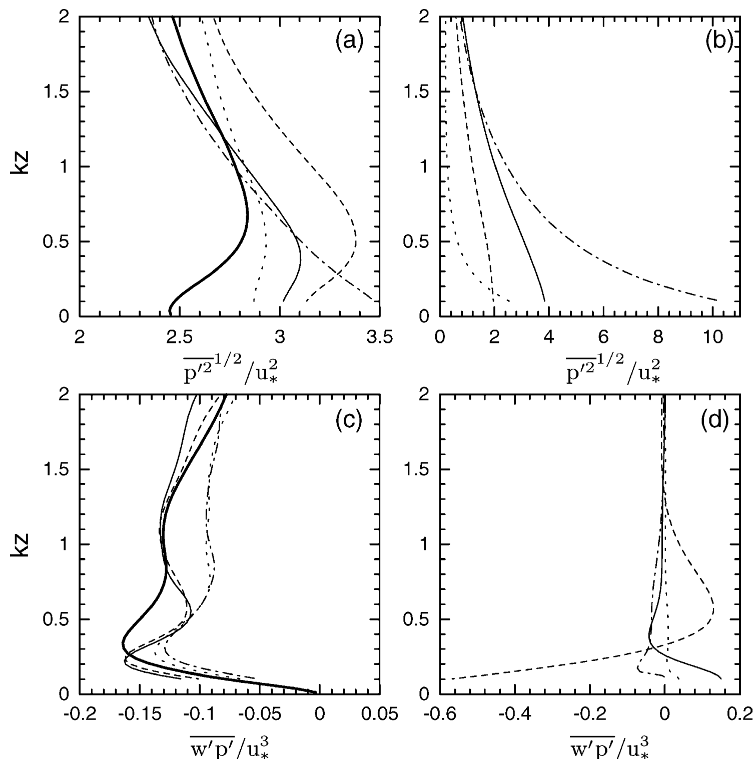

Fig. 3. Vertical profiles of root-mean-square pressure for (a) the turbulent contribution and (b) wave-induced contribution; vertical flux of pressure perturbation for (c) turbulent contribution and (d) wave-induced contribution. Lines are the same as in Fig. 2.

right panels of this figure. We notice that $\tilde{w}$ is symmetrically centered about the crest of the wave, 90 degrees out of phase with $\tilde{p}$. Since $\tilde{w}$ and $\tilde{p}$ are symmetrical and out of phase, the net $\tilde{w}\tilde{p}$ is very small despite large $\tilde{w}$ and $\tilde{p}$-values. The slight shift towards the crest of the maximum $\tilde{w}$ results in a small, but negative net value of $\overline{\tilde{w}\tilde{p}}$. For the slow-wave case, $\overline{\tilde{w}\tilde{p}}$ is larger than for the other cases; negative at the surface, and positive above $kz \approx 0.3$ and then changing sign again at $kz \approx 1.5$. Thus, $\overline{\tilde{w}\tilde{p}}$ (and also $\overline{\tilde{u}\tilde{w}}$, not shown) changes sign around or slightly above the critical layer. This is a consequence of the critical layer, which strongly influences $\tilde{w}$ and weakly impacts $\tilde{p}$ (Fig. 5). Above the critical layer, the vertical variances ($\overline{\tilde{w}}$) are shifted almost 90 degrees towards the wind resulting in a flow pattern resembling the stationary case (see figures 14 and 15 in Sullivan and McWilliams, 2002).

3.2. Kinetic energy budgets

To gain further insight into how turbulent and wave-induced kinetic energy (KE) is generated, transported, and dissipated, kinetic energy budgets are investigated for the total perturbation, wave-induced perturbation and the turbulent perturbation in the following sections. The KE budget in Section 3.2.1 is the sum of the turbulent and wave-induced perturbations. In Section 3.2.2, the KE budgets for the wave perturbation and turbulent perturbation are investigated separately.

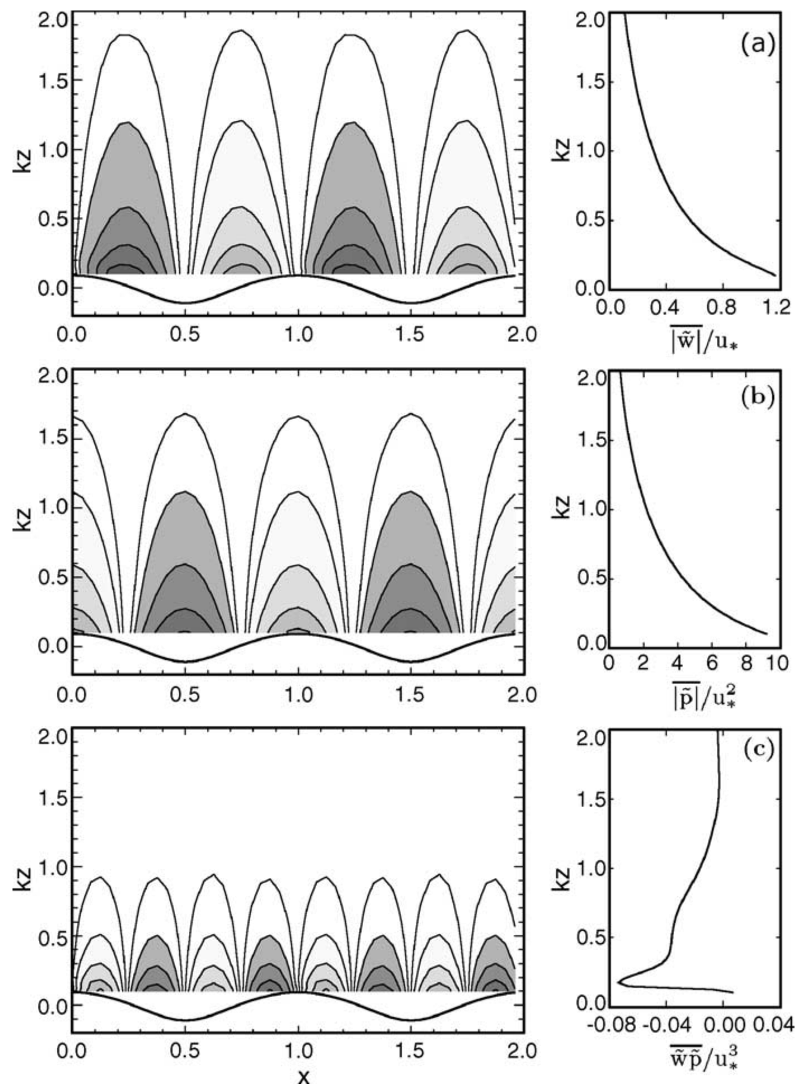

Fig. 4. Normalized wave-correlated fields of (a) $\tilde{w}/u_*$, contours ($\pm 0.2, \pm 0.4, \pm 0.8, \pm 1.2, \pm 1.6$), (b) $\tilde{p}/u_*^2$, contours ($\pm 1.5, \pm 3, \pm 6, \pm 10, \pm 14$) and (c) $\tilde{w}\tilde{p}/u_*^3$, contours ($\pm 1, \pm 3, \pm 6, \pm 10, \pm 14$), for the very fast-wave case ($c/u_* = 22.7$). The dark contours represent positive values and light negative values. The magnitude of the wave-integrated value is shown on the right.

3.2.1. Kinetic energy budget for the total perturbation

For statistically stationary and neutrally stratified conditions, the KE budget for the total perturbation is:

$$\underbrace{-\overline{u_i u_j}\frac{\partial U_i}{\partial x_j}}_{P} - \underbrace{\frac{\overline{\partial u_j e}}{\partial x_j}}_{T_\mathrm{t}} - \underbrace{\frac{1}{\rho}\frac{\overline{\partial u_i p}}{\partial x_i}}_{T_\mathrm{p}} + \underbrace{\frac{1}{2}\upsilon\frac{\overline{\partial^2 u_i^2}}{\partial x_j^2}}_{T_\mathrm{v}} - \underbrace{\overline{\upsilon\left(\frac{\partial^2 u_i}{\partial x_j}\right)^2}}_{\in} = 0 \tag{4}$$

where $e = \frac{1}{2}\overline{u_i^2}$ is the KE for the total perturbation. The physical interpretation of the terms is that P is the mechanical production of total KE from the mean flow, T_t is transport

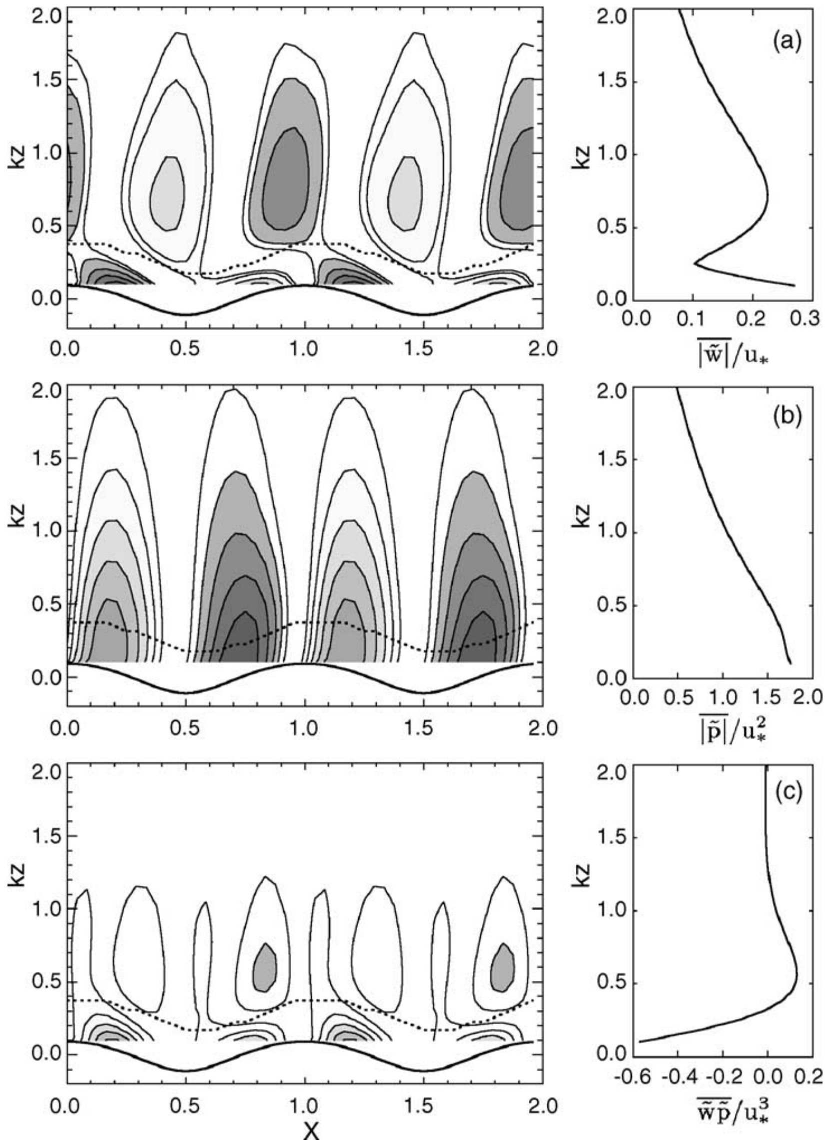

Fig. 5. As Fig. 4, but for the slow-wave case ($c/u_* = 7.8$). Contours are (a) ($\pm 0.15, \pm 0.2, \pm 0.3, \pm 0.4, \pm 0.5$), (b) ($\pm 0.8, \pm 1.2, \pm 1.6, \pm 2.0, \pm 2.4$) and (c) ($\pm 0.2, \pm 0.5, \pm 0.8, \pm 1.1, \pm 1.4$). The dotted line represents the height of the critical layer.

of KE by the turbulent eddies/wave perturbations, T_p is transport of total KE by pressure perturbation, T_v is transport by molecular diffusion, which can generally be neglected in the atmosphere and $\in$ is molecular rate of dissipation. All terms are computed directly from the DNS data and the residual of the terms is expected to be zero. In our flat case, the residual is very small and the results are similar to previous DNS (Spalart, 1988). Due to interpolation effects between the flat and curvy coordinate systems, the residual for the wavy cases is slightly larger, but it is significantly smaller than the other terms in the budget. The terms in the budgets are scaled with v/u_* and plotted against kz (also z^+ in Fig. 6a).

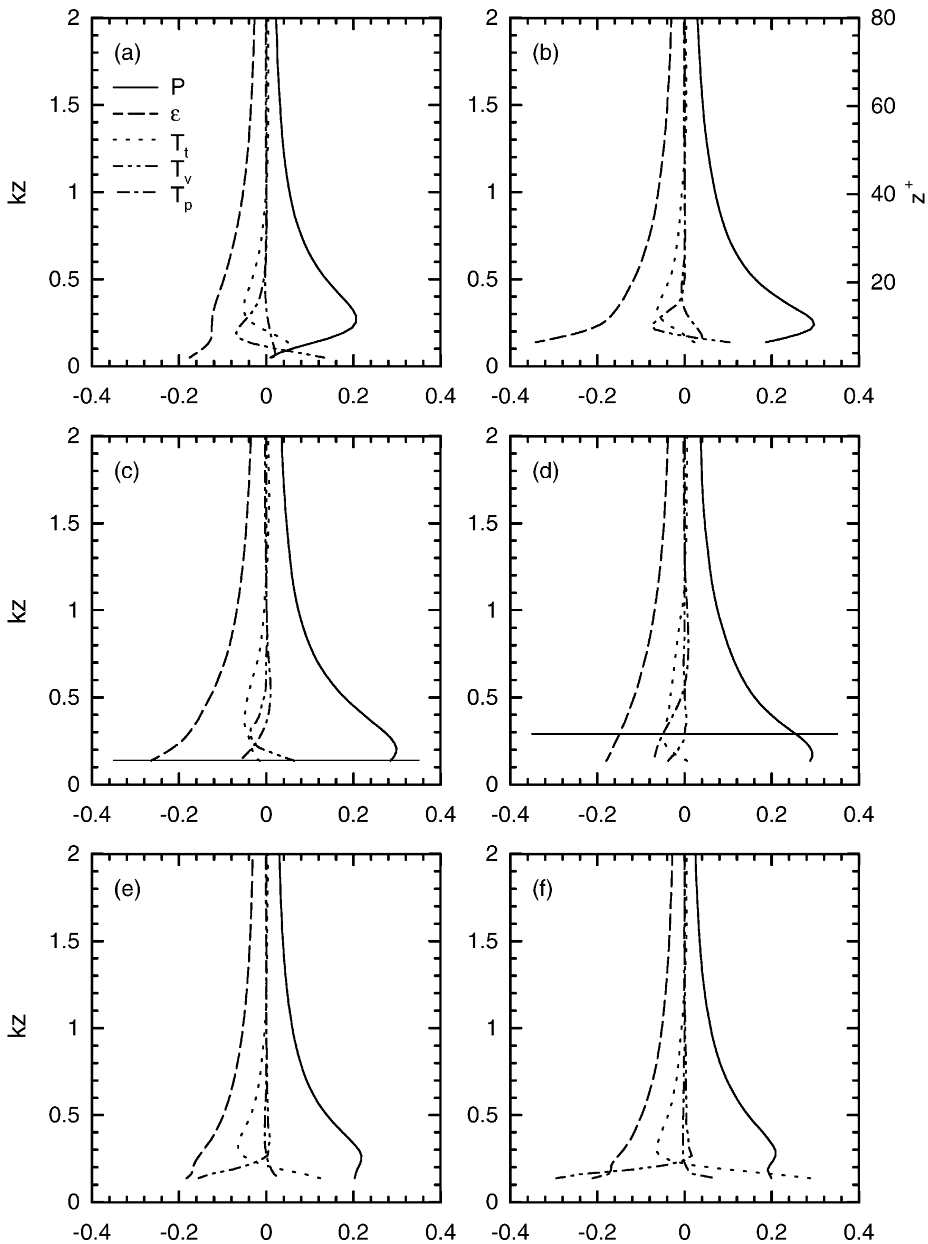

Fig. 6. Kinetic energy budget for the total perturbation for six neutral cases. For a (a) flat surface, (b) stationary wavy surface ($c/u_* = 0$), (c) very slow waves ($c/u_* = 3.9$), (d) slow waves ($c/u_* = 7.8$), (e) fast waves ($c/u_* = 16.2$) and (f) very fast waves ($c/u_* = 22.7$). Solid thin lines in (c) and (d) denote the approximate average height of the critical layer.

The KE budget for the total perturbation for six cases is shown in Fig. 6. The budget for the flat case (Fig. 6a) agrees well with other flat-wall DNS (Mansour et al., 1988; Spalart, 1988). The production and dissipation dominate the turbulent KE budget, and above $kz = 1$ they mainly balance. Below $kz = 1$, T_t is of increasing importance, transporting turbulence both to the surface and to higher levels. Closer to the surface (below $kz = 0.5$) T_p and T_v are increasingly important.

The stationary case with a wavy surface (Fig. 6b) differs from the flat, production is larger and dissipation is significantly larger, especially at the surface. Near the surface, pressure transport is slightly larger and the stationary wavy surface acts as a rougher surface producing more KE, which is dissipated locally.

Fig. 6c and d illustrate two cases where a critical layer is present near the surface. The critical layer mainly influences T_p, which is negative around and below the critical layer (this strong influence on T_p can also be seen from Fig. 3d where $\overline{\tilde{w}\tilde{p}}$ changes sign at about the height of the critical layer). The viscous transport is smallest for the cases with slow waves, which can be explained by the effective increase in surface roughness for slower waves (see z_0^+ in Table 1). When comparing cases with fast and very fast waves (Fig. 6e and f show $c/u_* = 16.2$ and 22.7, respectively), the most striking feature is the large increase in turbulent and viscous transport (T_t and T_v) near the surface. T_v is the largest sink near the surface and decreases to small values at $kz \approx 0.25$. T_p is small, except for right at the surface. Production and dissipation are similar to the flat case above the near-surface region.

Variance budgets can also be calculated for the u^2-, v^2- and w^2-components separately. In these budgets, an additional term appears (the redistribution term, $\phi_{ii} = \overline{\frac{p}{\rho}\frac{\partial u_i}{\partial x_i}}$), which moves energy between the different components. It is interesting to note that the redistribution of energy from the direction of the mean wind to the less energetic components is significantly larger for slow waves than the other cases below $kz = 0.75$ (in Fig. 7, u^2- and w^2-components are shown). This implies that the process of transporting energy from the mean-wind direction to the vertical and crosswind directions (making the turbulence more isotropic) is more efficient for slow waves. This partly explains why the variance is relatively low in the horizontal direction and large in the vertical direction in Fig. 2 for slow waves.

3.2.2. *Kinetic energy budget for the wave-induced and turbulent perturbations*

Next, we analyze the kinetic energy budget for the wave-induced (WKE) and turbulent (TKE) perturbations (for a derivation of these equations see Reynolds and

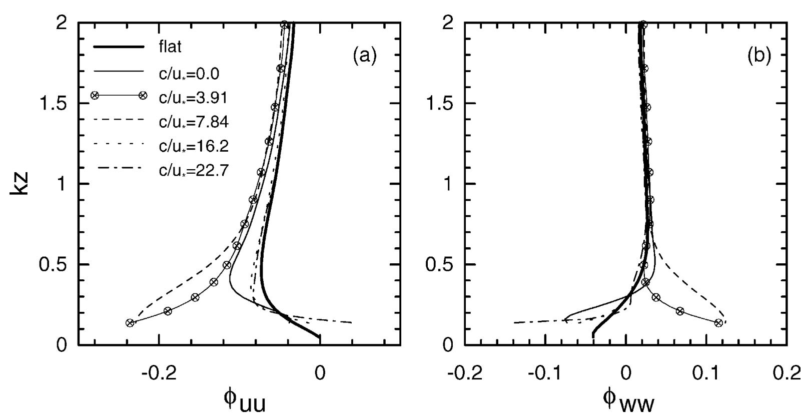

Fig. 7. Pressure redistribution term for (a) u-component and (b) w-component for six different cases.

Hussain, 1972):

$$\underbrace{-\overline{u_i u_j}\frac{\partial U_i}{\partial x_j}}_{\tilde{P}} - \underbrace{\overline{\frac{\partial \tilde{r}_{ij}\tilde{u}_i}{\partial x_j}}}_{\tilde{T}_{\mathrm{w}}} + \underbrace{\overline{\tilde{r}_{ij}\frac{\partial \tilde{u}_i}{\partial x_j}}}_{W_{\mathrm{t}}} - \underbrace{\overline{\tilde{u}_i\frac{\partial \tilde{R}_{ij}}{\partial x_j}}}_{\tilde{T}_{\mathrm{R}}} - \underbrace{\overline{\frac{\partial \tilde{u}_i \tilde{p}}{\partial x_i}}}_{\tilde{T}_{\mathrm{p}}} + \underbrace{\frac{1}{2}v\frac{\partial^2 \overline{\tilde{u}_i^2}}{\partial x_j^2}}_{\tilde{T}_{\mathrm{v}}} - \underbrace{v\overline{\left(\frac{\partial \tilde{u}_i}{\partial x_j}\right)}}_{\tilde{\epsilon}} = 0, \tag{5}$$

$$\underbrace{-\overline{\frac{1}{2}\tilde{u}_j\frac{\partial\langle u_i' u_i'\rangle}{\partial x_j}}}_{A_{\mathrm{w}}'} - \underbrace{\overline{u_i' u_j'}\frac{\partial U_i}{\partial x_j}}_{P'} - \underbrace{\overline{\tilde{r}_{ij}\frac{\partial \tilde{u}_i}{\partial x_j}}}_{W_{\mathrm{t}}} - \underbrace{\overline{\frac{\partial u_i' u_i'}{\partial x_j}}}_{T_{\mathrm{t}}'} - \underbrace{\overline{\frac{\partial u_i' p'}{\partial x_i}}}_{T_{\mathrm{p}}'} + \underbrace{\frac{1}{2}v\frac{\partial^2 \overline{u_i'^2}}{\partial x_j^2}}_{T_{\mathrm{v}}'} - \underbrace{v\overline{\left(\frac{\partial u_i'}{\partial x_j}\right)}}_{\epsilon'} = 0. \tag{6}$$

In the above expressions,

$$\tilde{r}_{ij} = \langle u_i' u_j'\rangle - \overline{u_i' u_j'} \qquad \text{and} \qquad \tilde{R}_{ij} = \tilde{u}_i\tilde{u}_j - \overline{\tilde{u}_i\tilde{u}_j},$$

$\tilde{r}_{ij}$ is the wave-induced turbulent Reynolds stress and $\tilde{R}_{ij}$ is the fluctuating part of the non-linear wave contribution to the Reynolds stress (Einaudi et al., 1984). The majority of the terms in Eqs. (5) and (6) have counterparts in Eq. (4). The new terms are: $\tilde{T}_{\mathrm{w}}$, redistribution of wave-induced turbulence, W_{t} is transport of energy between turbulence and wave perturbation and is present in both Eqs. (5) and (6). The non-linear term, $\tilde{T}_{\mathrm{R}}$, described in Einaudi et al. (1984), represents the oscillating part of the non-linear wave contribution to the Reynolds stress; it is a redistribution term and is generally considered to be small and is often neglected. The term A_{w}' is advection of turbulence by the wave; it is small, but not negligible. Our residual for the different cases is small and the WKE and TKE budgets are mainly closed. Generally, the terms in the WKE budget (Fig. 8) are smaller than in the TKE budget (Fig. 9), but still non-negligible. The production of wave energy is about 25% of total energy production from the mean flow below $kz = 0.4$ for the case with slow waves. Notice that for slow waves almost the entire pressure transport is in the wave perturbation, which agrees with Fig. 3c and d, where most of the gradient in $\overline{wp}$ is due to wave perturbation ($\overline{\tilde{w}\tilde{p}}$) for the slow-wave case.

There are major differences in the WKE budgets for varying c/u_* (see Fig. 8) with the stationary case noticeably different from the wavy cases. The production term for the stationary case is a sink of energy, i.e., energy is transported from wave perturbation to mean flow. This is also observed in Sullivan et al. (2000) (their figure 21) where $\overline{\tilde{u}\tilde{w}}$ for the stationary wavy surface is positive. Also, in the experimental study of Cheung and Street (1988), the surface layer beneath water waves shows a transport of energy from the wave perturbation to the mean flow. The source of WKE in our stationary case is due to a transport of energy from the TKE (W_{t}).

For the two slow-wave cases, we also see effects of the critical layer in the WKE budget; the production term is slightly negative above the critical layer and thus similar to flow above a stationary wavy surface. For slow waves, both production and turbulence-wave interaction (W_{t}) are energy sources near the surface and the pressure term transports it from the near-surface region to higher levels. The largest W_{t} term is found for the very slow and stationary cases. For fast waves, notice that the largest source of energy near the surface is the

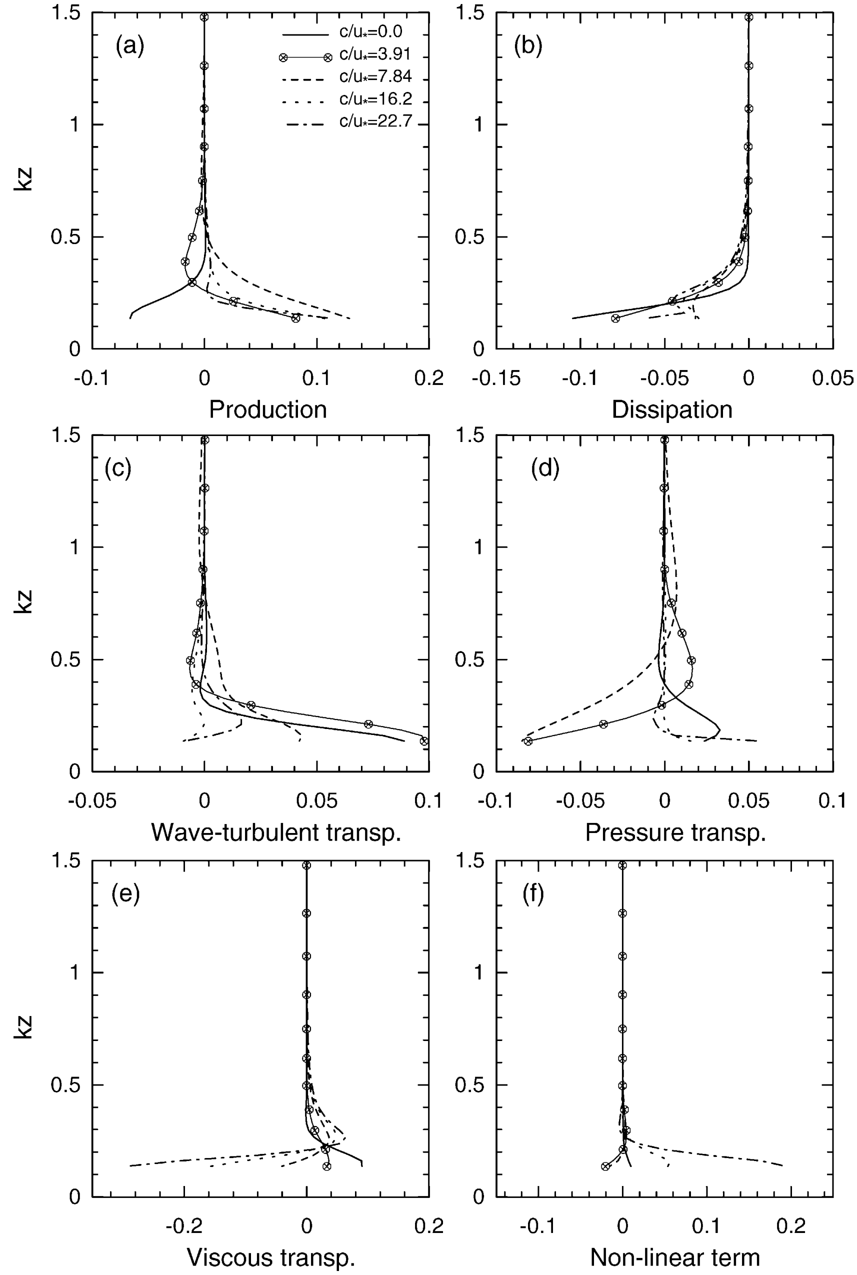

Fig. 8. Terms in the wave kinetic energy budget. (a) Production of wave-induced kinetic energy, $\tilde{P}$, (b) dissipation, $\tilde{\epsilon}$, (c) wave–turbulent transport, W_t, (d) pressure transport, $\tilde{T}_p$, (e) viscous transport, $\tilde{T}_v$ and (f) non-linear wave-wave interaction, $\tilde{T}_R$,

non-linear term ($\tilde{T}_R$ Fig. 8f) and the major sink is viscous diffusion ($\tilde{T}_v$, Fig. 8e). Since there exist very few previous investigations about the interaction between turbulence and wave perturbation over moving surface waves, we have chosen to relate some of the parameters with investigations of other types of flow including turbulence-wave interactions. The non-linear wave–wave interaction term, $\tilde{T}_R$, is also present in the turbulence-gravity wave study

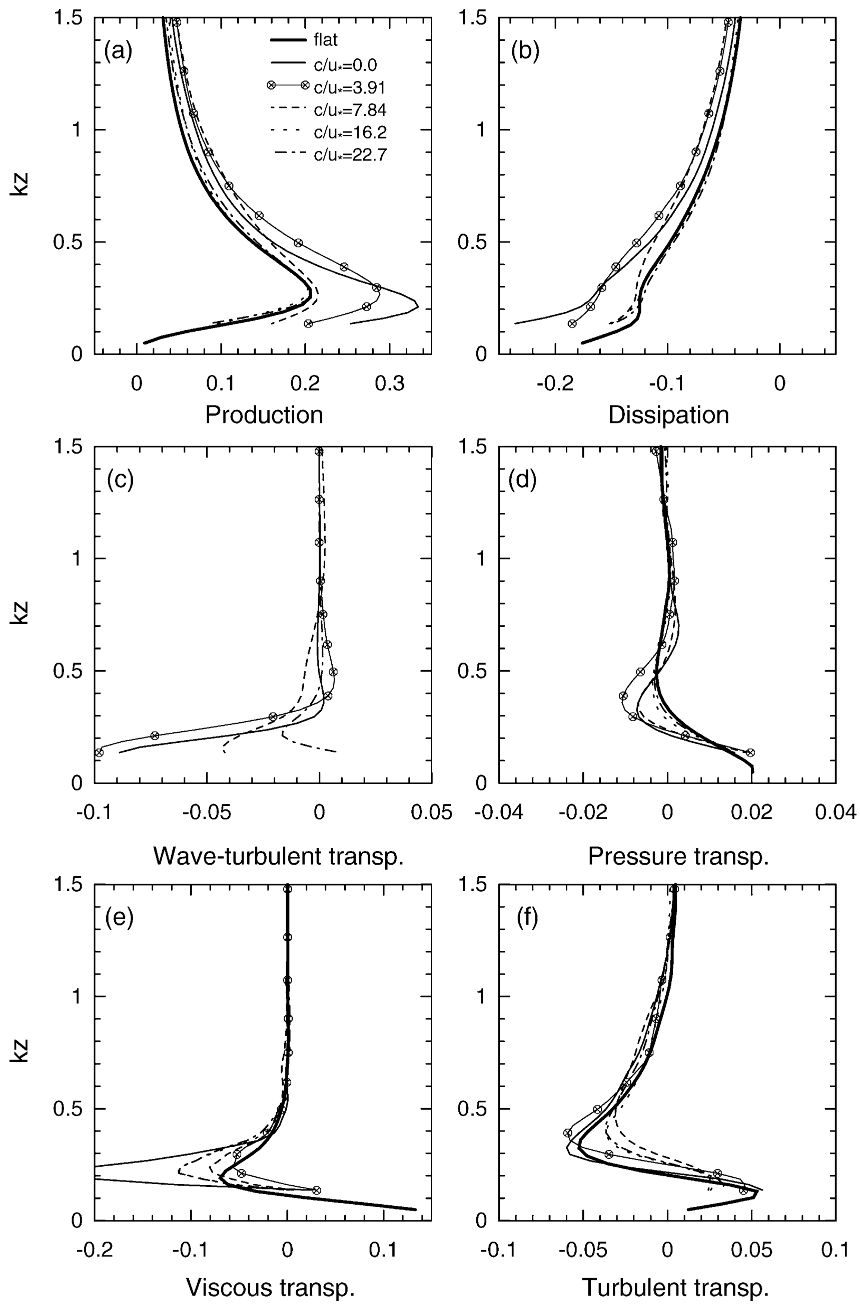

Fig. 9. Terms in the turbulent kinetic energy budget. (a) Production of turbulent kinetic energy, P', (b) dissipation of turbulent kinetic energy, $\in'$, (c) wave-turbulent transport, W_t, (d) pressure transport, T'_p, (e) viscous transport, T'_v and (f) turbulent transport, T'_t.

of Finnigan and Einaudi (1981), where it is described as a wave velocity transport, the counterpart of turbulent transport in the turbulent budget. In Finnigan and Einaudi (1981), $\tilde{T}_R$ can be both a sink and a source term. Production of wave energy from the mean flow as well as pressure transport is small for the fast-wave cases. The W_t term is relatively small, but of increasing importance for faster waves (i.e., larger for $c/u_* = 22.7$ than for

$c/u_* = 16.2$). It is frequently assumed that the dissipation of wave-energy is negligible (Liu and Merkine, 1976; Makin and Mastenbroek, 1996), which is an acceptable assumption in atmosphere and laboratory data, but for the DNS data the dissipation is of the same order as the production term in the WKE budget.

The different cases have a more similar budget for the TKE (Fig. 9), where also the flat case is included for comparison. It is interesting to note that the negative production of WKE for the stationary surface is compensated by about 30% larger production of TKE for the stationary surface than for the flat case. This extra production is, to a large extent, dissipated locally. In all cases, the turbulent transport as well as the pressure transport is similar to the flat case. The viscous transport gives an important contribution for $kz < 0.4$; it is larger for flat and stationary wavy surface than the other cases.

The assumption is sometimes done that the transport terms (referring to the turbulent and pressure transport terms) can be neglected in modeling wave–atmosphere interaction (Makin and Kudryavtsev, 1999). The DNS simulations indicate that this is a valid assumption above $kz = 1$, but that they should be included closer to the surface (Fig. 9).

3.2.3. Wave turbulence transport term

One of the most interesting terms in the wave and turbulent kinetic energy budgets is the transport between the organized wave components and the background turbulence, W_t. Due to measurement difficulties, this term is often assumed to be negligible (Cheung and Street, 1988). On the other hand, this term is assumed to dominate the energy balance for the organized motions studied in Reynolds and Hussain (1972). When analyzed, this transport is mostly directed from wave perturbation to the turbulent field (Liu and Merkine, 1976; Hsu et al., 1981; Makin and Kudryavtsev, 1999). This direction of transport is often assumed, based on a similarity to the turbulence energy cascade, where energy is usually transported from large to small scales. In this study, we find that the transport is mainly in the opposite direction, from the turbulent field to the wave perturbation, i.e., from smaller to larger scales. In order to shed light on this energy exchange process, we examine the different components of the transport term, W_t.

There are four dominant components in the wave-turbulence transport term, namely:

$$W_{t1} = \overline{\tilde{r}_{uu}\frac{\partial \tilde{u}}{\partial x}}, \qquad W_{t2} = \overline{\tilde{r}_{uw}\frac{\partial \tilde{w}}{\partial x}}, \qquad W_{t3} = \overline{\tilde{r}_{ww}\frac{\partial \tilde{w}}{\partial z}}, \quad \text{and} \quad W_{t4} = \overline{\tilde{r}_{uw}\frac{\partial \tilde{u}}{\partial z}} \tag{7}$$

Fig. 10 shows profiles of the various terms and their sum (W_t) for four different cases. W_{t1} represents the transport of wave-induced horizontal variance in the horizontal direction, it is the second largest contributor for most of the cases. With our definition, a negative sign implies transport of KE from the wave perturbation to the turbulence, a positive sign is transport from turbulence to the wave perturbation. In all cases but the stationary, W_{t1} represents negative transport. This can be compared with the laboratory data of Hsu et al. (1981) for equilibrium waves. They also obtain negative W_{t1} up to $kz \approx 0.7$. In Liu and Merkine (1976) (when modeling a turbulent shear layer with a super-imposed large-scale wave), W_{t1} is negative near the surface, but positive at higher levels, which does not agree with our results or with the data of Hsu et al. (1981).

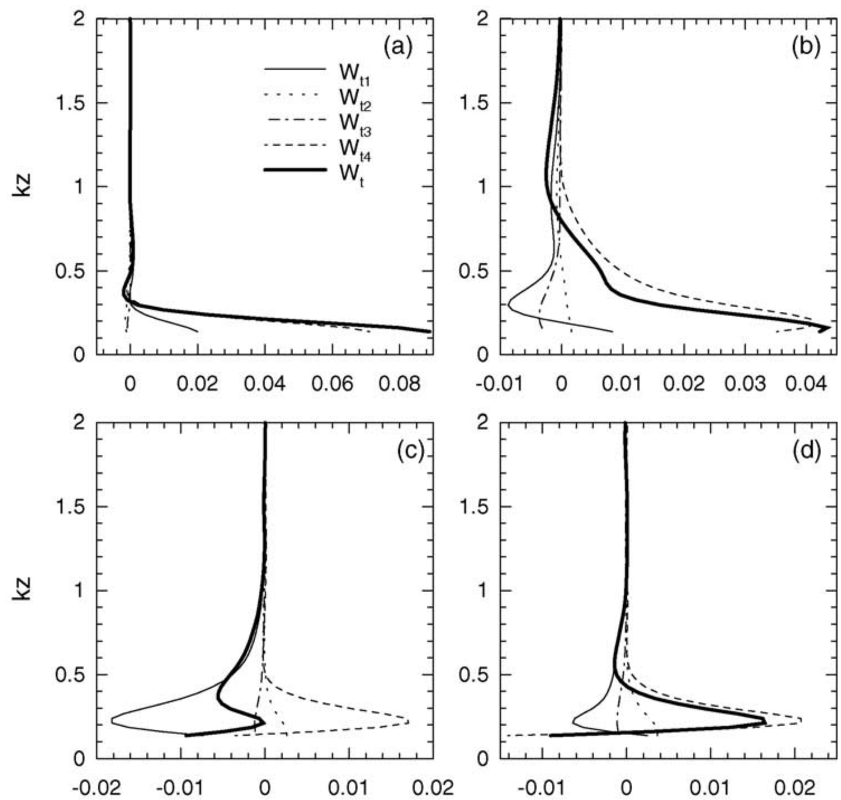

Fig. 10. The transport of energy between wave and turbulence. Positive data means transport from turbulence to wave perturbation. Thick line is the sum of the terms, thin solid is W_{t1}, dotted is W_{t2}, dash-dotted is W_{t3} and dashed is W_{t4}. The cases are (a) stationary wavy surface ($c/u_* = 0$), (b) slow waves ($c/u_* = 7.8$), (c) fast waves ($c/u_* = 16.2$) and (d) very fast waves ($c/u_* = 22.7$).

W_{t2} is small and slightly positive and W_{t3} is slightly negative. Both W_{t2} and W_{t3} have little impact on the resulting wave-turbulent transfer, and both are in qualitative agreement with the results of Hsu et al. (1981) and Liu and Merkine (1976).

W_{t4}, the analogue to the Reynolds stress term $(\overline{u'w'}\frac{\partial U}{\partial z})$, is positive for our flow, giving a transport of energy from turbulence to the wave perturbation. This is opposite to the findings of Hsu et al. (1981) and Liu and Merkine (1976).

In our flow, it is mainly the balance between the W_{t1} and W_{t4} that generates net wave-turbulent transport. For the case with well-developed waves (Fig. 10c), the balance between W_{t1} and W_{t4} results in a small net transport (from wave perturbation to turbulence). For slow waves as well as very fast waves, W_{t4} dominates and there is a significant net transport of energy from the turbulence to the wave perturbation.

There are important differences between the work of Hsu et al. (1981), Liu and Merkine (1976) and the present study that perhaps can explain the observed differences. Liu and Merkine (1976) examine the interactions between a large-scale structure and fine-grained turbulence in a free shear flow; this is not a boundary layer flow, as in our case. The work of Hsu et al. (1981) is similar to our study but is conducted at a higher Reynolds number with relatively well-developed waves. They also analyze the data using a wave-following coordinate system. It is interesting to note that in the DNS investigation of Papavassiliou and Hanratty (1997) over a flat surface, the transport of energy was also found to be upscale from the turbulence to the large-flow structure. Papavassiliou and Hanratty (1997) consider a plane Couette flow, with a Reynolds number slightly lower than ours ($Re = 2660$). Similar to the present work, their large-scale perturbation energy transfer from the turbulence to the secondary flow is due to an opposite relation between Reynolds stresses and the corresponding velocity gradients. This is explained by the fact that the secondary motion affects the turbulence and changes the Reynolds stresses in a way that can cause a supply of energy to the secondary flow.

Spatial (x, z) contours of W_{t1} and W_{t4} are shown in Figs. 11 and 12. Contours of $\tilde{r}_{ij}$, $\frac{\partial \tilde{u}_i}{\partial x_j}$ and the total term $\left(\tilde{r}_{ij}\frac{\partial \tilde{u}_i}{\partial x_j}\right)$ are shown. Vertical profiles of integrated values of the fields are also shown for $|\tilde{r}_{ij}|$ and $\left|\frac{\partial \tilde{u}_i}{\partial x_j}\right|$ and the resulting product, $\tilde{r}_{ij}\frac{\partial \tilde{u}_i}{\partial x_j}$

For W_{t1} and the slow-wave case (Fig. 11), the wave-induced turbulent Reynolds stress in the along-wind direction ($\tilde{r}_{uu}$) has its maxima (upward) centered over the troughs and minima (downward) at the crests near the surface. The critical layer generates strongly tilted secondary maxima shifted along the wind towards the crest of the waves (minima over the troughs). The horizontal gradients in the along-wind direction have minima at the windward side of the wave and maxima at the leeward side. Due to the strong tilt of the maxima in turbulent Reynolds stress ($\tilde{r}_{uu}$) at the critical layer, we have large negative values of W_{t1}. Near the surface, this term is slightly positive since the minima in turbulent Reynolds stress ($\tilde{r}_{uu}$) at the crests of the waves are larger than the maxima at the troughs.

For the fast- and very fast-wave cases (Fig. 12 shows the fast-wave case), the maxima/minima of horizontal turbulent Reynolds stress ($\tilde{r}_{uu}$) are centered over the crests/troughs and the tilt decreases with increasing wave age; at $c/u_* = 22.7$ there is no tilt or secondary maxima. The minima in horizontal gradients $\left(\frac{\partial \tilde{u}}{\partial x}\right)$ at the windward side of the wave is slightly stretched out over the crest of the wave, as a result of the orbital velocities. This expansion of horizontal gradients $\left(\frac{\partial \tilde{u}}{\partial x}\right)$ over the crests for fast waves results in a positive contribution near the surface to W_{t1}. W_{t1} is largest for well-developed waves and is smaller for very fast waves (except near the surface). For slow waves, the secondary peak is out of phase with the gradients, and the main effects can be seen at the critical layer.

The sign and size of the wave-turbulence transport is sensitive to the phase relationship between wave-induced turbulent Reynolds stresses ($\tilde{r}_{ij}$) and the gradients, and can change due to small shifts in the wave stresses. Near the surface, the effect of the surface orbital velocities on the vertical gradient are clearly observed for fast waves. W_{t4} is positive for our cases (except near the surface) and is largest for stationary or slow waves, since then the turbulent Reynolds shear stress of uw ($\tilde{r}_{uw}$) becomes larger. W_{t1} can be either positive or negative and for well-developed sea nearly balances W_{t4}, giving a small wave-turbulence transport. Thus, it is the tilt of the maxima/minima of horizontal turbulent Reynolds stress ($\tilde{r}_{uu}$) in combination with the strength of turbulent Reynolds shear stress ($\tilde{r}_{uw}$) that has the largest influence on the total W_t. This sensitivity to the phase of the wave-induced turbulent Reynolds stresses can explain the differences in W_t for different flows.

It is clear that the wave-turbulence transport is a significant contribution to the TKE and WKE budgets for some cases. This is especially true in the WKE budget where this

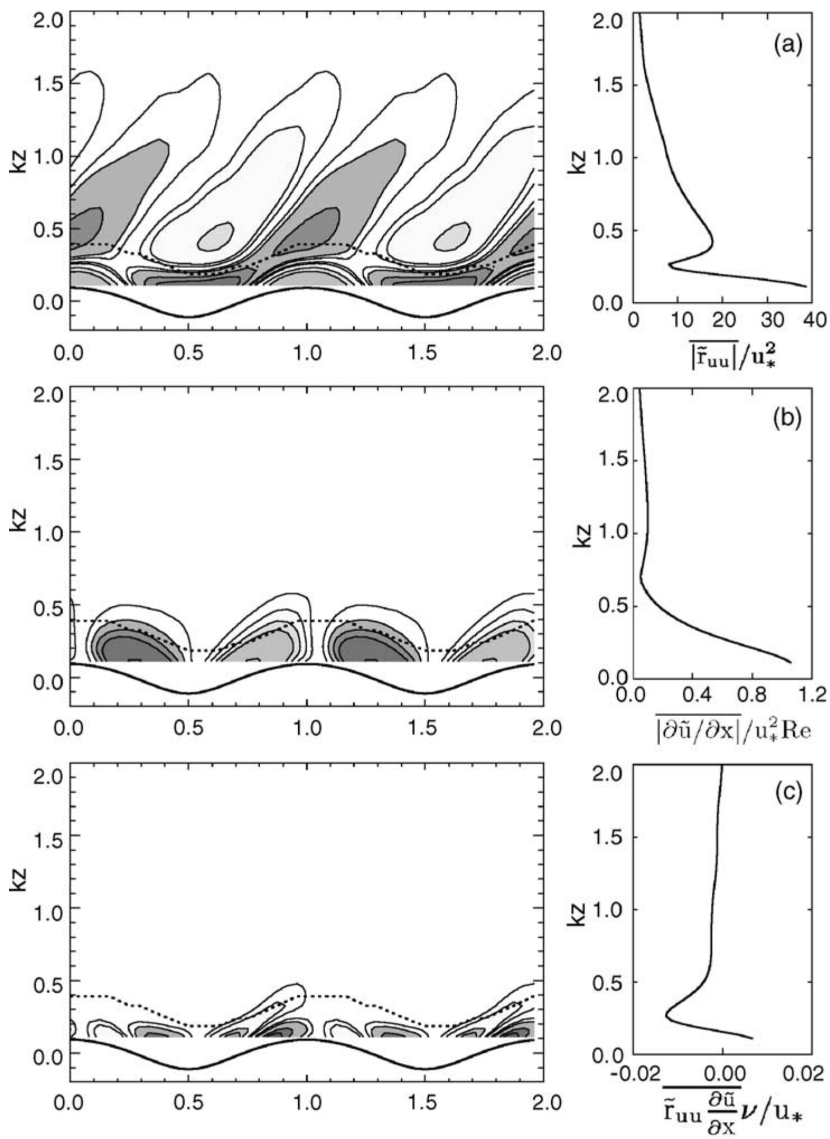

Fig. 11. Phase average of (a) $\tilde{r}_{uu}$, contours ($\pm0.2, \pm0.4, \pm1.0, \pm1.5, \pm2.5$), (b) $\frac{\partial\tilde{u}}{\partial x}$, contours ($\pm0.01, \pm0.02, \pm0.03, \pm0.04, \pm0.08$) and (c) W_{t1}, contours ($\pm0.02, \pm0.04, \pm0.08, \pm0.10$) for the case with slow waves ($c/u_* = 7.8$). The dark contours represent positive values and light negative values. The magnitude of the wave-integrated value is shown on the right. Dashed line shows the height of the critical layer.

term is the major source of energy for stationary waves and also for very slow waves (which resemble stationary waves above the critical layer). But also, for very fast waves it has a non-negligible contribution. When we are near a fully developed wave state the wave-turbulent transport is small. Most investigations examine a well-developed, mature sea and find a small or negligible wave-turbulence transport. That is in agreement with our data, since we see a relatively small transport of energy from wave perturbation to turbulent perturbation for a mature sea. The term is of increasing importance both for slower and faster waves and energy is then transported from turbulence to the wave-induced perturbation.

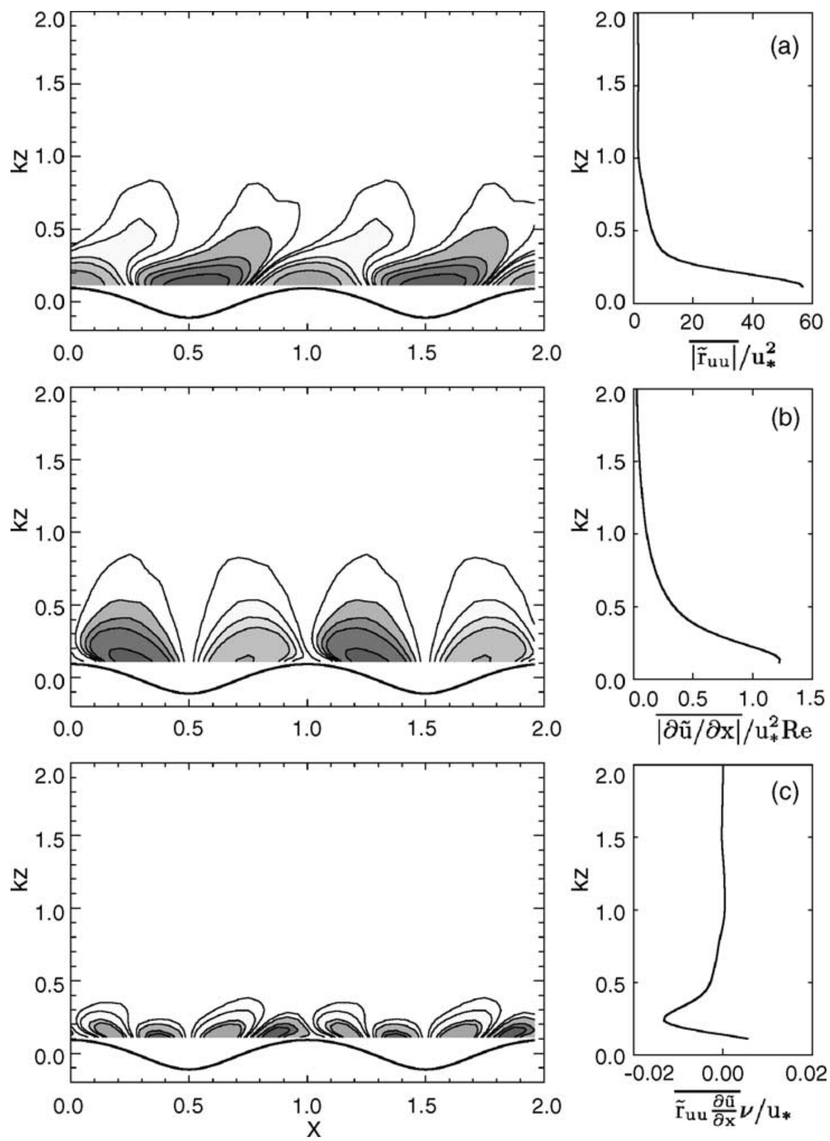

Fig. 12. Phase average of (a) $\tilde{r}_{uu}$, (b) $\frac{\partial\tilde{u}}{\partial x}$ and (c) W_{t1} for fast waves ($c/u_* = 16.2$). Contours as in Fig. 11.

4. Discussion

The present work has described some features of the turbulence structure and KE budgets in the flow over moving surface waves. It would be interesting to know how applicable the data are to atmospheric conditions over moving ocean waves. There are a number of differences including the idealized waveform in the DNS, with a single monochromatic wave, the absence of small-scale ripples, and no flow separation. These features are most important for slow waves. The present DNS have also a relatively low Reynolds number ($Re_* = 130$), and possible influence of viscous effects. According to traditional turbulence theories (Monin and Yaglom, 1973) the viscous sublayer is the region where the viscous stresses are considerably greater in magnitude than the Reynolds stresses, $z^+ < 5$, this corresponds to the region $kz < 0.1$ and is only very near the surface in our data. This estimate agrees well with the DNS simulations (see Sullivan et al. (2000), their figure 5). The intermediate region, where both viscous stresses and Reynolds stresses contribute, is $5 < z^+ < 30$ and corresponds approximately to $0.1 < kz < 0.7$. In this region we thus have important wave effects combined with effects of Reynolds stresses and viscous stresses. It can be difficult to distinguish between the different effects. However, one should remember that frequent viscous effects can be of importance also in atmospheric flows (for example, airflow over short waves or at low to moderate wind speeds) (Harris et al., 1996).

When looking at the results, there is a difference between DNS data and data with higher Reynolds number in the classification of the wavy surface. In Sullivan et al. (2000), young waves are defined as having positive pressure drag (or form stress) and old waves, negative pressure drag; the transition for the DNS data was found to be $c/u_{*|\mathrm{tr}} \approx 14$. This can be compared to second-order closure calculations where the limit is $c/u_{*|\mathrm{tr}} \approx 22$. According to Harris et al. (1996), the limit is $c/u_{*|\mathrm{tr}} \approx 30$ for atmospheric conditions. These different values indicate that the relation between the friction velocity and the phase speed of the waves determining the transition from slow to fast waves are dependent on Reynolds number and the roughness of the lower boundary. When c/u_λ is used as a criterion (where u_λ is the wind speed at one wave length above the surface), the agreement in wave-age classification between DNS and second-order closure data is significantly better (Sullivan et al., 2000). The scaling u_λ is, however, difficult to deduce from measured data.

When slow waves are present, the wind speed is often relatively high and the surface, rough. During these conditions, the differences compared to the DNS might be expected to be large. In Weng et al. (submitted for publication), the mean flow streamlines and the profiles of $\overline{uw}$ using second-order closure data are in qualitative agreement with the present DNS. A second-order closure model can thus, to a certain extent, reproduce the low Reynolds number DNS, despite the possible shortcomings in parameterization over a moving wavy surface and differences in Reynolds number. Harris et al. (1996) conclude from second-order closure modeling that a large change in Reynolds number does not greatly influence the magnitude of the velocity perturbations. Despite the similarities, some important differences between DNS and data with higher Reynolds number remain, including the height of the critical layer and the wave growth. The growth rate of waves from a second-order closure by Meirink and Makin (2000) are dependent on Reynolds number. This implies a different growth rate for DNS and second-order closures, and may also explain some of the scatter in experimental data (Plant, 1982). The growth rate is larger for lower Reynolds numbers. Including low Reynolds number effects in second-order closure models improves the agreement with laboratory data (Meirink and Makin, 2000) and also bring second-order closure results and DNS data closer together. The height of the critical layer is shifted to lower levels when the Reynolds number increases (Weng et al., submitted for publication). This can influence the vertical profiles, since the behavior of variances and fluxes often differ above and below the critical layer.

One expects the situation with fast waves to agree better with measurements than for slow waves. With fast waves, we do not need to consider very short waves on the sea surface (which are not included in the DNS) and the wind speed is often lower, which leads to lower Reynolds numbers. Also, there are no critical layer effects complicating the analysis near

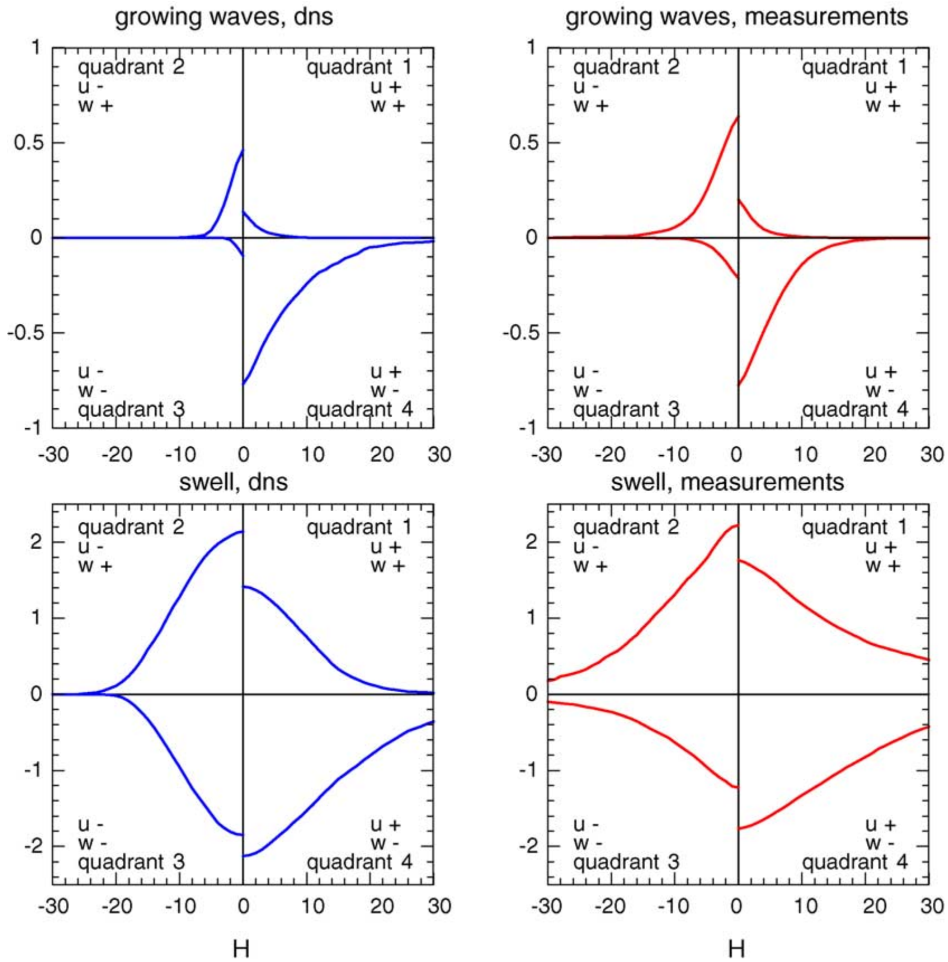

Fig. 13. Quadrant analysis for growing sea (upper) and swell (lower) from DNS (left) and measurements taken at Östergarnsholm in the Baltic Sea (right). The measurements are taken at 10 m above the sea surface. The DNS data is from $kz = 0.2$ for the case with growing sea $c/u_* = 7.84$ and swell $c/u_* = 22.7$.

the surface. For fast waves, there are some interesting similarities between the DNS and measured data, taken over the open ocean. In Fig. 13, quadrant analysis is shown for slow and fast waves for the DNS as well as from observations. The quadrant analysis separates the uw-flux into four quadrants depending on the sign of the two fluctuating components. The relative importance of events is estimated by determining the cumulative frequency distribution of the fluxes. Then, the fluxes are plotted as a function of the hole size, H, where large H represents large flux events. For $H = 0$, the sum of all quadrants is $= -1$. The measurement data, described by Smedman et al. (1999), are obtained from a mast at 10 m height located on the small island of Östergarnsholm in the Baltic Sea. The DNS data represent slow waves and very fast waves near the surface, $kz = 0.2$. It is interesting to note that the special features found for very fast waves in the atmosphere are also replicated in the DNS runs. The slow waves show a quadrant analysis similar to what can be expected, where the two quadrants responsible for the downward momentum flux (quadrants 2 and 4) dominate. For very fast waves, the contribution from each quadrant is significantly larger in both measurements and DNS. The large wave-induced events responsible for upward and downward transport of momentum thus exist both in the atmosphere and in the DNS with fast waves. These events are probably responsible for the high levels of turbulence found in the DNS and measurements. The phase shift between the u- and w-components results in very low vertical transport, despite the high turbulence levels.

There are also some major differences between the DNS data and atmospheric measurements during fast waves. For example, some of the terms in the TKE budget are different. The dominating pressure transport term found in studies from the Baltic Sea (Rutgersson et al., 2001) is not reproduced by the present DNS data. Differences between the DNS and measurements can be explained by several factors where the most important one probably is the limitation in wave age for the DNS-simulation. Over the open ocean, the friction velocity approaches zero and the wave-age parameter goes to infinity. This is not the case for the DNS, where also the 'very fast case' represents relatively limited wave-age conditions. In the atmosphere, there is also a development in time for the wave-turbulence interaction, i.e., the flow is not fully stationary, while in the DNS we have absolutely stationary conditions. The presence of synoptic- and meso-scale features also influence the measured data.

Parameters like wave growth or height of the critical layer from high Reynolds atmospheric conditions cannot be expected to be exactly reproduced by the DNS. Nevertheless, there are similar turbulent structures both for slow and fast waves and further insight would be obtained by investigating a wider range of wave conditions. DNS is thus a useful tool for investigating turbulent structures in the atmosphere above a wavy surface; however, not all parameters can be directly translated to atmospheric conditions.

5. Summary

Direct numerical simulations of airflow over a sinusoidal wavy surface with different wave conditions are analyzed. The data are separated into wave-induced and turbulent perturbations. We find large differences in the wave-induced and turbulent parts depending on the state of the waves. For the wave-induced contribution with fast waves, the horizontal and vertical variances are larger than for slow waves, as is also the case for the root-mean-square pressure. The wave signal is present in many fields up to 0.2λ and to even higher levels for faster waves. If we extrapolate our results to atmospheric conditions and waves of wavelength $\lambda = 60$ m, we would have a wave influence up to at least 12 m.

Despite the large variances for fast waves, the wave-induced vertical fluxes of momentum ($\tilde{u}\tilde{w}$) and pressure ($\tilde{w}\tilde{p}$) are small for well-developed and fast waves. This is because $\tilde{w}$ is almost 90 degrees out of phase with $\tilde{u}$ and $\tilde{p}$, respectively. The contribution of the turbulence part to the variances and fluxes differ across wave age. This implies that simply removing the effect of the wave by removing the wave-induced perturbations is not possible. The u-variance is smallest for slow waves, while the w-variance is largest. This is a consequence of the redistribution term in the variance budgets. Energy transport from u- to v- and w-components is significantly more efficient for slow waves than for fast. Slow waves have thus a much higher degree of isotropy near the surface than stationary and fast waves.

The quadrant analysis shows that for fast waves the vertical transport is controlled by a few large events, and that the fluxes are shifted from the usual quadrant 2 and quadrant 4 to larger contributions from all four quadrants. These large flux events are forced by the underlying fast waves. Wave-effects remain at higher levels for fast waves. For slow waves, significant critical layer effects can be seen with pronounced minima in low-speed quadrants at the critical layer. The structure above the critical layer is similar to that over a stationary wavy surface.

The kinetic energy budget for the total perturbation shows important wave effects. The production (as well as dissipation) increases for slow waves compared to a flat surface and the pressure transport term is of importance. For fast waves, turbulent and viscous transport dominates close to the surface. The kinetic energy budget, analyzed separately for wave perturbation and turbulent perturbation, shows that the energy transport is directed from the turbulence to the wave perturbation in the airflow, i.e., from smaller to larger scales, for most cases. The wave-turbulence transport is largest for slow waves and close to zero or even slightly directed from wave to turbulence for the well-developed cases. For fast waves, it is directed from turbulence to wave, but smaller in magnitude than for slow waves. This means that the underlying waves generate larger turbulence levels than at a flat surface, and this energy then feeds the wave perturbation. The size and direction of the wave-turbulence transport is shown to be very sensitive to the size, phase and tilt of the wave-induced turbulent Reynolds stresses ($\tilde{r}_{ij}$). Here, horizontal turbulent Reynolds stress ($\tilde{r}_{uu}$) shows the largest dependence on the wave age and height of the critical layer.

The redistribution of energy (return-to-isotropy) seems to be a key parameter, and for turbulence above slow waves the isotropy is much larger than during fast waves due to a more efficient redistribution.

Acknowledgments

The stay at NCAR for Anna Rutgersson was supported by STINT (Stiftelsen for internationalisering av hogre utbildning och forskning). Peter P. Sullivan was partly supported by the Office of Naval Research through the CBLAST initiative, contract no. N00014-00-C-0180. Ulf Hogstrom and Ann-Sofi Smedman are acknowledged for valuable comments on the manuscript.

References

Belcher, S.E., Hunt, J.C.R., 1998. Turbulent flow over hills and waves. Ann. Rev. Fluid Mech. 30, 507–538.

Cherukat, Y., Na, P., Hanratty, T.J., 1998. Direct numerical simulations over a fully developed turbulent flow over a wavy wall. Theor. Comput. Fluid Dyn. 11, 109–134.

Cheung, T.K., Street, R.L., 1988. The turbulent layer in the water at an air–water interface. J. Fluid Mech. 194, 133–151.

Donelan, M.A., Drennan, M.W., Katsaros, K.B., 1997. The air–sea momentum flux in conditions of mixed wind sea and swell. J. Phys. Oceanog. 27, 2099.

Drennan, M.W., Kahma, K.K., Donelan, M.A., 1999. On momentum and velocity spectra over waves. Bound. Layer Meteor. 92, 489–515.

Einaudi, F., Finnigan, J.J., Fua, D., 1984. Gravity wave turbulence interaction in the presence of a critical layer. J. Atmos. Sci. 41, 661–667.

Finnigan, J.J., Einaudi, F., 1981. The interaction between an internal gravity wave and the planetary boundary layer. Part II. Effect of the wave on the turbulence structure. Q. J. R. Met. Soc. 107, 807–832.

Harris, J.A., Belcher, S.E., Street, R.L., 1996. Linear dynamics of wind-waves in coupled turbulent air–water flow. Part 2. Numerical model. J. Fluid Mech. 308, 219–254.

Hristov, T.S., Miller, S.D., Friehe, C.A., 2003. Dynamical coupling of wind and ocean waves through wave-induced air flow. Nature 422, 55–58.

Hsu, C.-T., Hsu, E.Y., Street, R.L., 1981. On the structure of turbulent flow over a progressive water wave: theory and experiment in a transformed, wave-following co-ordinate system. J. Fluid Mech. 105, 87–117.

Hussain, A.K.M.F., Reynolds, W.C., 1970. The mechanics of an organized wave in turbulent shear flow. J. Fluid Mech. 41, 241–258.

Kawamura, H., Toba, Y., 1988. Ordered motion in the turbulent boundary layer over wind waves. J. Fluid Mech. 197, 105–138.

Kitaigorodskii, S.A., Donelan, M.A., 1984. Wind-wave effects on gas transfer. In: Brutsaert, W., Jirka, G.H., Reidel. (Eds.), Gas Transfer at Water Surfaces.

Komen, G., Cavaleri, L., Donelan, M., Hasselman, K., Hasselman, S., Janssen, P., 1994. Dynamics and Modelling of Ocean Waves. Cambridge University Press, Cambridge, 532 pp.

Kudryavtsev, V.N., Makin, V.K., Meirink, J.F., 2001. Simplified model of the air flow above waves. Bound. Layer Meteor. 100, 63–90.

Li, P.Y., Xu, D., Taylor, P.A., 2000. Numerical modelling of turbulent airflow over water waves. Bound. Layer Meteor. 95, 397–425.

Liu, J.T.C., Merkine, L., 1976. On the interactions between large-scale structure and fine-grained turbulence in a free shear flow. Part I. The development of temporal interactions in the mean. Proc. R. Soc. London A 352, 213–247.

Mansour, N.N., Kim, J., Moin, P., 1988. Reynolds-stress and dissipation-rate budgets in a turbulent channel flow. J. Fluid Mech. 194, 15–44.

Makin, V.K., Kudryavtsev, V.N., 1999. Coupled sea surface-atmosphere model 1. Wind over waves coupling. J. Geophys. Res. 104, 7613–7623.

Makin, V.K., Mastenbroek, C., 1996. Impact of waves on air–sea exchange of sensible heat and momentum. Bound. Layer Meteor. 79, 279–300.

Mastenbroek, C., Makin, V.K., Garat, M.H., Giovanangeli, J.P., 1996. Experimental evidence of the rapid distortion of turbulence in the air flow over water waves. J. Fluid Mech. 318, 273–302.

Meirink, J.F., Makin, V.K., 2000. Modelling low-Reynolds-number effects in the turbulent air flow over water waves. J. Fluid Mech. 415, 155–174.

Monin, A.S., Yaglom, A.M., 1973. Statistical Fluid Mechanics, vol. 1. The MIT Press, 769 pp. (English edition).

Papavassiliou, D.V., Hanratty, T.J., 1997. Interpretation of large-scale structures observed in a turbulent plane Couette flow. Int. J. Heat Fluid Flow 18, 55–69.

Plant, S.P., 1982. A relationship between wind stress and wave slope. J. Geophys. Res. 87, 1967.

Reynolds, W.C., Hussain, A.K.M.F., 1972. The mechanics of an organized wave in turbulent shear flow. Part 3. Theoretical models and comparisons with experiments. J. Fluid Mech. 54, 263–288.

Rutgersson, A., Smedman, A.-S., Hogstrom, U., 2001. Use of conventional stability parameters during swell. J. Geophys. Res. 106 (27), 117–127, 134.

Smedman, A., Högstrom, U., Bergström, H., Rutgersson, A., Kahma, K., Pettersson, H., 1999. A case-study of air–sea interaction during swell conditions. J. Geophys. Res. 104 (25), 833–925, 851.

Spalart, P.R., 1988. Direct simulation of a turbulent boundary layer up to $R_\theta = 1410$. J. Fluid Mech. 187, 61–98.

Sullivan, P.P., McWilliams, J.C., 2002. Turbulent flow over water waves in the presence of stratification. Phys. Fluids 14, 1182–1195.

Sullivan, P.P., McWilliams, J.C., Moeng, C.-H., 2000. Simulation of turbulent flow over idealized water waves. J. Fluid Mech. 404, 47–85.

Weng, W., Taylor, P.A., Sullivan, P.P. On turbulent and mean flow reynolds stress above sinusoidal waves. J. Phys. Ocean. submitted for publication.